Plastic Behavior of Glassy Polymers: Experimental and Theoretical Description Based on Three Different Approximations

Z. G. Pandermarakis, G. Spathis

Department of Applied Mathematics and Physical Sciences, Section of Mechanics, National Technical University of Athens, 5 Heroes of Polytechnion, GR-15773 Athens, Greece

Received 19 April 2004; accepted 5 January 2005
DOI 10.1002/app.21876
Published online in Wiley InterScience (www.interscience.wiley.com).

ABSTRACT: Three different models were used for the description of viscoelastic, yielding, and hardening stages of the mechanical behavior of a network polymer. As a representative response we get unidirectional loading test at a wide range of strain rates with the appearance of a distinct yielding point, strain softening, and strain hardening. The present analysis shows that Rubin's kinematics formulation appears to have some benefits in contrast to the other two approximations. © 2005 Wiley Periodicals, Inc. J Appl Polym Sci 97: 2032–2046, 2005

Key words: mechanical properties; viscoelastic properties; viscoplasticity; yielding; modeling

INTRODUCTION

Generally speaking, almost all polymers exhibit an interesting "peculiarity" (due to transition phenomena): they could expose every kind of behavior like that of a glassy solid, an elastic elastomer, or a viscous liquid according to temperature, time scale of testing, and history of the specimen or, in a most astonishing manner, all these appearances could coexist in a more complicated response as a result of specific excitation conditions. The description of each behavior demands different approximation and mathematical formulation.[1,2]

With regard to linear viscoelasticity in polymers, Boltzmann's superposition principle[2] or, equivalently, general differential equations can be used as constitutive equations for stress–strain relations.[2–4] In the second case, the description of viscoelastic response could arise through models constructed from elastic springs and viscous dashpots. As far as nonlinear viscoelasticity[2,4,5,6,7] develops, which frequently is exhibited by most polymers, we should be faced with the help of approximated theories based on a molecular, rheological, and/or empirical basis, like Schapery representation,[2] the Kohlraush–Williams–Watts equation,[4] stress-clock function,[7] or Eyring's viscous theory.[2]

Temperature, strain rate, pressure, and some other parameters affect significantly the general mechanical behavior of polymers and so their plastic response.[1,2] But, although polymers cannot be considered ideal plastic materials, their yielding behavior could, in a first approximation, be faced through the theories of ideal plasticity as long as these parameters remain constant and conditions are selected so adiabatic heating does not take place. Through experimental testing work, it has been confirmed that the modified Mises criterion finds extensive application in the case of polymers.[2] In many cases nonlinear viscoelasticity could be used to approximate the polymer yield process,[1] e.g., through the relation of Schapery and the KWW equation for the representation of a wide relaxation time distribution (spectrum). Correspondingly, Eyring's viscous theory could be extended to describe also the process of yield, but the obscure terms and the lack of strain softening terms are some of its disadvantages. Argon[8] has suggested that the yield process corresponds essentially to the overcoming of molecular chain elastic interactions with its neighborhood, so the resistance in plastic deformation at the yielding point arises mainly from these interactions between molecules.

The exhibited inhomogeneity during yielding is also an interesting feature of glassy polymers under mechanical response. The inhomogeneous nature of shear deformations through yielding with the appearance of characteristic sheared regions led Bowden and Raha[9] in the development of a rate-activated process model using the basic principles of dislocation theory. From a different point of view G'Sell and Jonas,[10] using the well-known expression of Orowan for the plastic strains in metals, attain an accurate representation of stress–strain curves and all accompanied fea-

Correspondence to: G. Spathis (gspathis@central.ntua.gr).

tures of polymers like strain softening, transition phenomena, physical aging, and softening after cycling loading.

In this study we tried to describe a three-dimensional mechanical response of glassy polymers using three different approximations. At the beginning the Boyce, Parks, and Argon model (BPA)[11–13] was presented and adjusted appropriately whereas uniaxial tension and compression tests were carried out for its calibration in a wide strain rate range. A specific material was used with representative behavior that under strain conditions of tests exhibited distinctive yielding peak followed by strain softening and hardening at the final stage. For the strain rate dependence of yielding stress, Argon's and Eyring's relations were applied, whereas the hardening stage was approximated using a three-chain model. For the initial viscoelastic part, appropriate linear viscoelastic models were applied but nonlinear viscoelastic approximations were used and investigated as well. In the BPA model the stress drop is connected with the variation of athermal shear resistance to which we accept a progressive decrease versus developed plastic strains. Finally, the dependence of yielding stress from loading conditions was given through the corresponding dependence from hydrostatic pressure. Applying G'Sell and Jonas'[10] model we supposed that the density of nucleated plastic sites is increased linearly with stresses using Gilman and Johnston's[10] approximation. Besides the comparison of the last two approximations, a different theory—which is based on Rubin's kinematics formulation initially developed for time evolution of microstructure variables in metals—was attempted in the plastic behavior of glassy polymers. In the present analysis we considered the rate of plastic rotations at the beginning to be zero and we followed the same approximations as the BPA models for the different stages. The application of these considerations in the examined polymer gave interesting results not only for this specific material but also for the applied models.

EXPERIMENTAL

Materials—Preparation and manufacturing of specimens

In obtaining a representative mechanical response of a polymer matter, we used as material reference a network polymer, with relatively low glass transition temperature. This is obtained by an epoxide system with low molecular weight (<700), which is prepared from the diglycydyl ether of diphenol A. The three-dimensional stereochemical formula is given in Figure 1. The weight ratio of the two constituents used was 100:50 resin/hardener. The attentive mixing in the above-mentioned ratio followed adequate degassing in vacuum pump. Consequently, for the case of tensile testing, the casting was carried out in appropriate-shape molds so as the resulting casts have the form of thin plates with thickness of 2.5 mm. From these specific plates dog-bone-shape specimens were manufactured with 1.5 cm width and 6.5 cm gauge length. This was followed by an annealing of specimens at 45°C for 12 h so as to complete the curing and also to remove the remaining stresses.

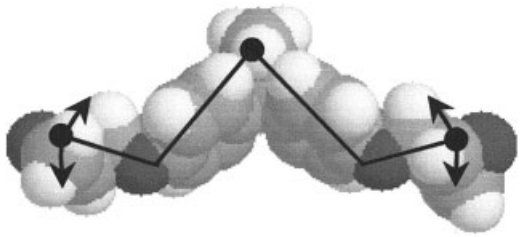

Figure 1 Three-dimensional stereochemical formula of DGEBA. Determination of molecular parameters.

To perform unidirectional compression tests, appropriate cylinder specimens were prepared with diameter 1.5 cm and height 2 cm. For this reason, casting was carried out in appropriate cylinder silicon molds. From the extracted casts we shaped specimens in the desire dimensions. After the manufacturing of specimens, their tempering at 45ºC for 12 h is followed so as to complete the postcuring procedure and also to remove the remaining stresses.

Uniaxial extension loading

The tests were carried out with an Instron type 1121 extension testing machine with capacity of 1 ton. During the tests the values of the exerted loads and imposed extensions were recorded through a suitable interface. At the same time direct electronic storage of the received values was carried out through appropriate software installed into the testing machine. For accurate receiving measurement of strains at the initial stage we used strain gauges so the exact determination of the elastic response of materials was extracted.

To obtain true stress–strain curves the following relations were applied:

$$\sigma = \frac{P}{A_0}(1 + \varepsilon_n) = \sigma_n(1 + \varepsilon_n) \tag{1a}$$

and

$$\varepsilon = \ln\left(1 + \frac{\Delta l}{l_0}\right) = \ln(1 + \varepsilon_n), \tag{1b}$$

where σ and ε are the true stresses and strains and σ_n and ε_n are the corresponding nominal values, A_0, l_0 are the initial values of cross section area and length of specimen and Δl is the change of length during defor-

TABLE I
Yielding Stresses via Strain Rates for Tension Loading

$\Delta l/\Delta t$ (mm/min)	0.1	0.2	0.5	1	2	5
$\dot{\varepsilon}$ (10^{-4}/s)	0.22	0.44	1.11	2.2	4.4	11.1
σ_y (MPa)	41.5	44.5	48.1	50.6	55.9	62.1

mation. At the same time the true strain rate also is calculated through the relation

$$\dot{\varepsilon} = \frac{d\ \ln(1+\varepsilon_n)}{dt} = \frac{\dot{\varepsilon}_n}{1+\varepsilon_n}. \tag{2}$$

The crosshead speed of the loading machine varied from 0.1 to 10 mm/min resulting in a corresponding range of strain rates ($\dot{\varepsilon}$) of specimens from 2.2×10^{-5} to 2.2×10^{-3}/s (see Table I). The corresponding yielding stresses (σ_y) are also included in Table I.

In Figure 2 true stress–strain curves are presented for uniaxial tension loading and for various strain rates. As it is shown from this plot the increasing strain rate doesn't result in a significant differentiation on the initial viscoelastic stage of the diagram, with the linearity remaining generally at the same bounds, followed by a monotonous increase in yielding stress. In Figure 4 the variation of observed yield stress in respect to the logarithmic strain rate is shown, exhibiting–without loss of accuracy—an almost linear correlation between the two quantities:

$$\sigma_y = 5.14\ \ln\ \dot{\varepsilon} + 95.7\ (\text{MPa}). \tag{3}$$

This result is in agreement with Eyring's and Argon's approximations. In Eyring's consideration an admission has been made that the applying stress causes a flowing in polymers analogous to viscous theory. According to this theory, the combined effect of stress τ and thermal energy kT, where k is the Boltzmann constant, results in the distraction and reconstruction of bonds between molecules. If we consider an action in the direction of loading and another one in the opposite direction, we find that the strain rate will be given via appearing stress, from the relation

$$\dot{\gamma} = \dot{\gamma}_0 \exp\left(\frac{-\Delta H_a + \upsilon_a \tau_y}{kT}\right), \tag{4}$$

where ΔH_a is the activated enthalpy, υ_a is activated volume, and $\dot{\gamma}_0$ is the fundamental rate factor. The preceding equation can be accordingly written as

$$\sigma_y = \alpha + \beta\ \ln\ \dot{\varepsilon}, \tag{5}$$

making use of the suitable relations which correlate τ_y with σ_y and γ_y with ε_y.

The above dependence is in agreement with the experimental results of Expression [3], identifying the

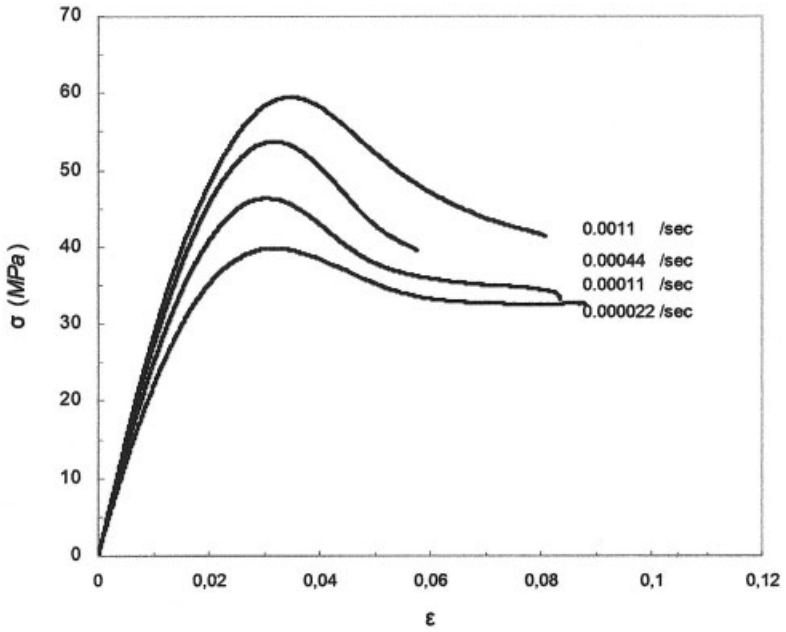

Figure 2 True stress–strain curves under unidirectional tension loading at various strain rates. Material: epoxy resin.

TABLE II
Yielding Stresses via Strain Rates for Compression Loading

$-\Delta l/\Delta t$ (mm/min)	0.5	1	2	5	10
$-\dot{\varepsilon}$ (10^{-3}/s)	0.36	0.73	1.5	3.7	8.2
$-\sigma_y$ (MPa)	70.5	72.7	75.5	78.4	84.3

conclusion that the yield stress is proportional to the logarithm of the strain rate.

From an other point of view, based on Argon's theory we obtain a similar expression for shear yield stress $\tau_{y,}$

$$\tau_y = \frac{G}{8}\left[1 - \frac{kT}{G\omega^2 r^3}\ln\left(\frac{\dot{\gamma}_0}{\dot{\gamma}}\right)\right]^{6/5}, \qquad (6)$$

where G is the shear modulus, r the molecular radius, and ω is the angular rotation of molecular segments.

Making the approximation that the exponent 6/5 of the right part of this equation is near to unity, the preceding relation turns to Expression [3], a fact that shows the intensive similarity of the two models. This fact results in the conclusion that their differences aren't remarkable for the present deformation processes. So these two relations appear to be equivalent for our study.

As is obvious from the stress–strain plots, the strain that reveals the maximum stress—ield stress—doesn't change remarkably and fluctuates around the value of 3.2%. Similar behavior to yield stress variation appears also for the yield stress drop in the strain softening stage. The increase of strain rate leads to a corresponding spread of stress drop at the range of 15 to 25%. Also a relatively small change of ductility that fluctuates from 8.4 to 5.6% is observed, whereas the final fracture stress is also affected, appearing with generally greater values: from 36.6 to 53.2 MPa (Fig. 2).

Compression loading

The tests were carried out on a Instron TT-CM (5 ton) testing machine. Collecting the experimental data of imposing loads and displacements results in a similar behavior to that in tension loading tests. The calculation of true stresses and strains plots has been made using the expressions applied in the corresponding case of tension tests.

As in unidirectional tension loading, the study of material mechanical behavior in a wide range of strain rates has been carried out. In Table II the corresponding results of yield stresses for various rates are also included.

In Figure 3 we present the true stress–strain curves for unidirectional compression loading and for various strain rates. In Figure 4 we plot the variation of yield stress with logarithm of strain rate in unidirectional compression loading. We notice directly that the linear dependence of these two quantities is described from the relation

$$\sigma_y = 4.26 \ln \dot{\varepsilon} + 103.6 \text{ (MPa)} \qquad (7)$$

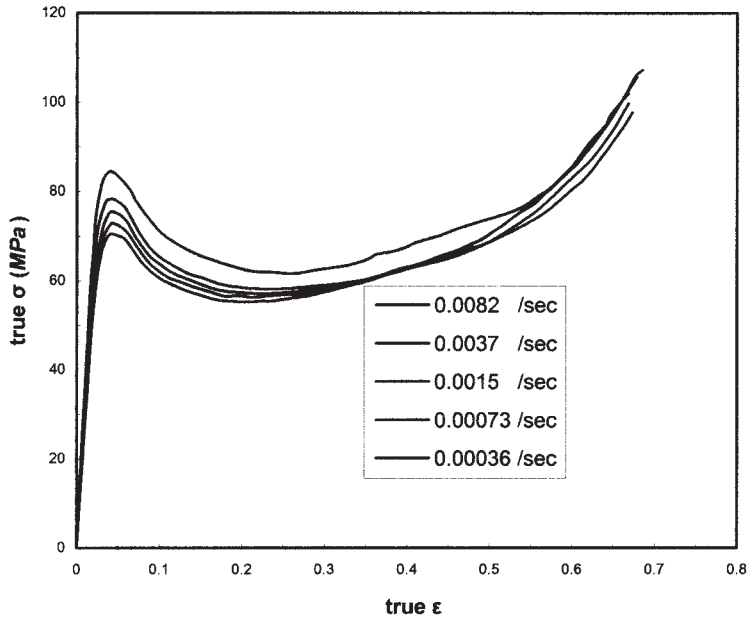

Figure 3 True stress–strain curves under unidirectional compression loading of epoxy rein for various strain rates.

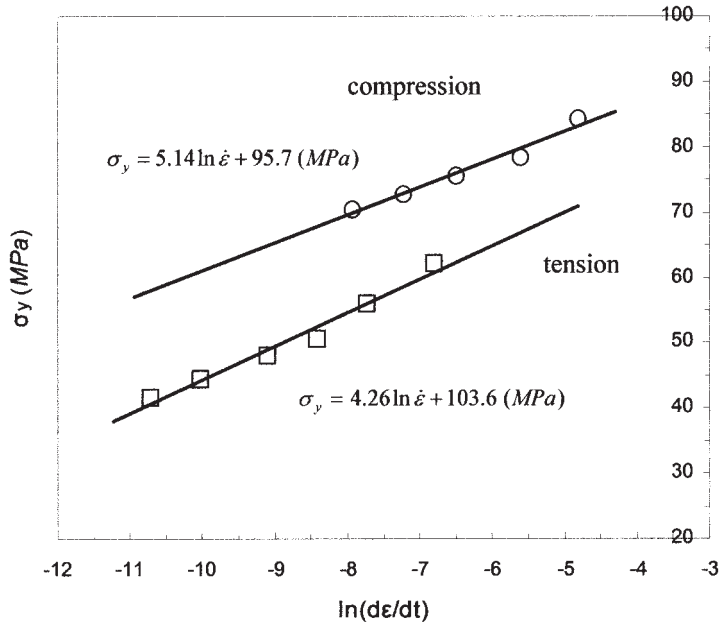

Figure 4 Variation of yielding stress via strain rate under tension and compression unidirectional loading.

On the other hand the yield strain doesn't appear to change noticeably and fluctuates around the value of 4.3%.

After the stage of yield, a characteristic drop of the imposed stress appears. But a question arises: is this an intrinsic strain softening or does it appear to be due to adiabatic heating? Because this drop appeared also for very small strain rates, the case of adiabatic heating is excluded. Consequently, the strain softening, especially in the case of compression loading, should result from a pure intrinsic feature of the material.

A stabilization of imposed stresses follows the appearance of a relative minimum. Finally, in the last stage, a continuous increase of imposed stresses appears to the point of fracture. In this stage—the hardening stage—we notice uniformity in material behavior at different rates. This fact expresses the intrinsic hardening that the material exhibits due to the developing strains, consequently leading gradually to strong resistances (greater than that of yield stresses) until, finally, failures. Its description is approximated with great accuracy using the rubber elasticity theory. Indeed, a part of the mechanical work that is supplied in a polymeric material during its deformation is spent for its internal energy changes and the other part is used for its entropic changes. In glassy polymers, during cooling, the statistical random chain model is preserved below the glass transition temperature. So the orientation, which takes place during the imposing of large deformations, provokes effective changes in molecular conformations, which result in entropic changes. Understandably, the strain hardening that appears in polymeric materials, after the stage of yielding at final stages of deformation, could be attributed to the entropic variations of chains. Although in thermoplastic materials the application of the relevant theory demands the introduction of the concept of entanglements and the number of active chains, it is not a necessity for the case of crosslinking polymers, where a constant three-dimensional lattice appears.

Finally, the ductility of the tested specimens (~68%) doesn't seem to be affected seriously as happened with the fracture stress, which fluctuates for all rates around the value of 105 MPa, with a small variation.

Summarizing the above observations of the two kinds of loading tests of this study, we result to the following conclusions. The development of ductile behavior, at least in a wide spread of rates at the testing temperature, results in obtaining large deformations of the tested material with local maximum to appear in the stress–strain diagrams.

More specifically, the initial linear response of the stress–strain diagram is followed from a nonlinear response that is completed with the appearance of a characteristic maximum yield limit. In the following, a significant softening with a stress drop stabilizing in values obviously lower from yield stress is obtained. In compression tests the development of strong hardening is obvious, whereas in tension loading tests this effect appeared only for very low strain rates. Also, in the case of tension loading due to geometrical conditions the material exhibited is less ductile. Due to the cross-section reduction and from the existence of stress singularities around its structural imperfections, true stresses arise rapidly, leading to a failure mechanism under small deformation. From the other hand, during the application of compression loads, localized deformations aren't observed, so the material strongly resists even under large deformations. In this stage the stresses gradually increase, a fact that is recorded as

an entropic hardening due to the development of plastic deformations.

But the most crucial difference is the fact that the yield stresses during compression are lightly but systematically greater than that of the tension loading case. This phenomenon could easily be explained as a consequence of yield stress dependence from hydrostatic stress. The modified law of von Mises criterion can then be applied:

$$(\sigma_1 - \sigma_2)^2 + (\sigma_2 - \sigma_3)^2 + (\sigma_3 - \sigma_1)^2 = 6(\tau_y^0 + \mu p)^2 \tag{8}$$

or

$$\tau_y = \tau_y^0 + \mu p, \tag{9}$$

so the application of compression stresses will result in the increasing of appeared characteristic limit for yield, while under the application of tension loads, the corresponding limit will be decreased.

In the following, we attempt to describe all previous features of polymer mechanical response using three different approximations.

APPROXIMATION MODELS

Simulation of Boyce–Parks–Argon (BPA)[11]

Constitutive formulation

In the case of unidirectional loading the deformation tensor **F** is given by

$$\mathbf{F} = \begin{bmatrix} \lambda_1 & 0 & 0 \\ 0 & \lambda_2 & 0 \\ 0 & 0 & \lambda_3 \end{bmatrix} = \begin{bmatrix} \lambda & 0 & 0 \\ 0 & \frac{1}{\sqrt{\lambda}} & 0 \\ 0 & 0 & \frac{1}{\sqrt{\lambda}} \end{bmatrix}, \tag{10}$$

where $\lambda = \lambda_1$ is the main stretching to the direction of imposed load where the isovolume condition has been taken into account. Then the Cauchy stress tensor will be given as

$$\mathbf{T} = \begin{bmatrix} \sigma - B_1 & 0 & 0 \\ 0 & -B_2 & 0 \\ 0 & 0 & -B_3 \end{bmatrix}. \tag{11}$$

In the above expressions B_i are the back stresses—due to entropic hardening—while σ is the stresses in the absence of back stresses.

The hydrostatic stress pressure will be

$$\mathbf{P} = \frac{1}{3}(\mathrm{tr}\,\mathbf{T})\mathbf{I} = \begin{bmatrix} p & 0 & 0 \\ 0 & p & 0 \\ 0 & 0 & p \end{bmatrix}, \tag{12}$$

where

$$p = \frac{\sigma - (B_1 + B_2 + B_3)}{3} \tag{12a}$$

so the deviatoric tensor $\mathbf{T}'$ will then be given as follows:

$$\mathbf{T}' = \mathbf{T} - \mathbf{P} = \begin{bmatrix} \frac{2[\sigma - (B_1 - B_2)]}{3} & 0 & 0 \\ 0 & -\frac{\sigma - (B_1 - B_2)}{3} & 0 \\ 0 & 0 & -\frac{\sigma - (B_1 - B_2)}{3} \end{bmatrix}. \tag{13}$$

The equivalent shear stress can be calculated now from the sequel equation:

$$\tau = \left[\frac{1}{2}\,\mathrm{tr}(\mathbf{T}')^2\right]^{1/2} = \left[\left(\frac{4\sigma^2}{9} + \frac{\sigma^2}{9} + \frac{\sigma^2}{9}\right)\frac{1}{2}\right]^{1/2} = [\sigma - (B_1 - B_2)]/\sqrt{3}. \tag{14}$$

The constitutive equation of stresses for large deformations, which is given by

$$\mathbf{T} = \frac{1}{J}\,\mathbf{L}^e \ln \mathbf{F}^e, \tag{15}$$

can be simplified in the case of isotropic material in unidirectional load as follows

$$\sigma = E \ln \lambda_e \tag{16}$$

or

$$\sigma = E\varepsilon_{el}. \tag{17}$$

So the equivalent shear stress will be given finally by

$$\tau = [\sigma - (B_1 - B_2)]/\sqrt{3} = [E \ln \lambda_e - (B_1 - B_2)]/\sqrt{3} = [E\varepsilon_{el} - (B_1 - B_2)]/\sqrt{3}. \tag{18}$$

The symmetric part $\mathbf{D}^{\mathrm{P}}$ of the plastic velocity gradient tensor $\mathbf{L}^{\mathrm{P}}$ is obtained from the associate flow rule as follows,

$$\mathbf{D}^p = \dot{\gamma}^p \mathbf{N}, \tag{19}$$

where the rate of plastic strains according to Argon's theory will be

$$\dot{\gamma}^p = \dot{\gamma}_0 \exp\left\{-\frac{A\tilde{s}}{T}\left[1-\left(\frac{\tau}{\tilde{s}}\right)^{5/6}\right]\right\}, \quad (20)$$

with $\tilde{s}$ expressing the athermal shear resistance depending on the hydrostatic pressure and rate of plastic deformation:

$$\tilde{s} = s + ap \quad (21)$$

$$\dot{s} = h\left(1-\frac{s}{s_{ss}}\right)\dot{\gamma}^p \quad (22)$$

with

$$s_0 = \frac{0.077\mu}{1-\nu}. \quad (23)$$

The s_{ss} is the limiting value of s in stable condition and h is the slope of yield drop with plastic strain. From the multiple decomposition of the deformation gradient tensor **F** and the additive relation for the velocity gradient **L** we obtain

$$\dot{\varepsilon}_{tot} = \dot{\varepsilon}_{el} + \dot{\varepsilon}_{pl} \quad (24)$$

or

$$\dot{\varepsilon}_{el} = \dot{\varepsilon}_{tot} - \dot{\gamma}^p/\sqrt{3} \quad (25)$$

$$\dot{\varepsilon}_{el} = \dot{\varepsilon}_{tot} - \frac{1}{\sqrt{3}}\dot{\gamma}_0 \exp\left\{-\frac{A\tilde{s}}{T}\left[1-\left(\frac{\tau}{\tilde{s}}\right)^{5/6}\right]\right\}. \quad (26)$$

Combining Eqs. [25] and [20] resulted in the following relation for the rate of elastic strains:

$$d\varepsilon_{el} = \left\{\dot{\varepsilon}_{tot} - \frac{1}{\sqrt{3}}\dot{\gamma}_0 \exp\left\{-\frac{A\tilde{s}}{T}\left[1-\left(\frac{\tau}{\tilde{s}}\right)^{5/6}\right]\right\}\right\}dt, \quad (27)$$

$$\tilde{s} = s + ap, \quad (28)$$

$$ds = \left[h\left(1-\frac{s}{s_{ss}}\right)\dot{\gamma}^p\right]dt, \quad (29)$$

$$p = \frac{1}{3}\,\mathrm{tr}\,\boldsymbol{T}, \quad (30)$$

$$s_0 = 0.077\mu/1-\nu, \quad (31)$$

$$\tau = [\sigma - (B_1 - B_2)]/\sqrt{3}, \quad (32)$$

and

$$\sigma = E\varepsilon_{el}, \quad (33)$$

where the constants $\dot{\gamma}_0$, A, E, α, h, s_{ss}, and v should be determined.

The elasticity modulus E and Poisson's ratio ν resulted directly from the stress–strain curves in small deformations, while $\dot{\gamma}_0$ and A are determined easily through the construction of diagrams $\ln \dot{\gamma}^p$ via $[\tau/(s_0 + ap)]^{5/6}$ as they are given in Figure 5a and b for tension and for compression, respectively, (see Ref. [11]). The values that resulted for $\dot{\gamma}_0$ and A are included in Table III. The corresponding figures could verify the linear dependence of the two quantities that simply confirm the preceding analysis. Finally, the determination of B_1 and B_2 will be given in the following paragraph.

Strain softening and hardening

In the approximation of the post yield region of stress–strain curves, where a characteristic stress drop is observed even for true stress–strain curves, a basic suggestion will be undertaken. In the BPA model a homogenization was tried for a general inhomogeneous behavior during strain softening of polymers. So we adopt the assumption that the macroscopically observed stress drop was due to the progressive diminishing of the athermal shear resistance via appearing plastic strains. The rule that governs this variation of athermal shear resistance s will be given from the relation

$$\frac{d}{dt}s = h\left(1-\frac{s}{s_{ss}}\right)\frac{d}{dt}\gamma^p, \quad (34)$$

where h is the slope of stress drop and s_{ss} is the final preferable value of s.

The rate h of stress drop via the deformation could be calculated through

$$h \approx \frac{\Delta s}{\Delta \gamma^p}\left(\frac{1}{1-\frac{s_0}{s_{ss}}}\right). \quad (35)$$

From stress–strain curves for compression, we notice that the percentage of stress drop $\Delta\sigma/\sigma_{max}$, where $\Delta\sigma = \sigma_{max} - \sigma_{min}$ during the stage of softening is relatively independent of strain rate and so the ratio s_{ss}/s_0 is considered to remain constant. Comparing now maximum and minimum yield stresses at this stage, we obtain

$$s_{ss}/s_0 = 0.825 \quad (36)$$

or

$$s_{ss} = 0.825 \times s_0. \quad (37)$$

The dependence of yielding with pressure could also be concluded easily from the above equations modifying the athermal shear resistance s by taking into account the pressure dependence as in Eq. [21].

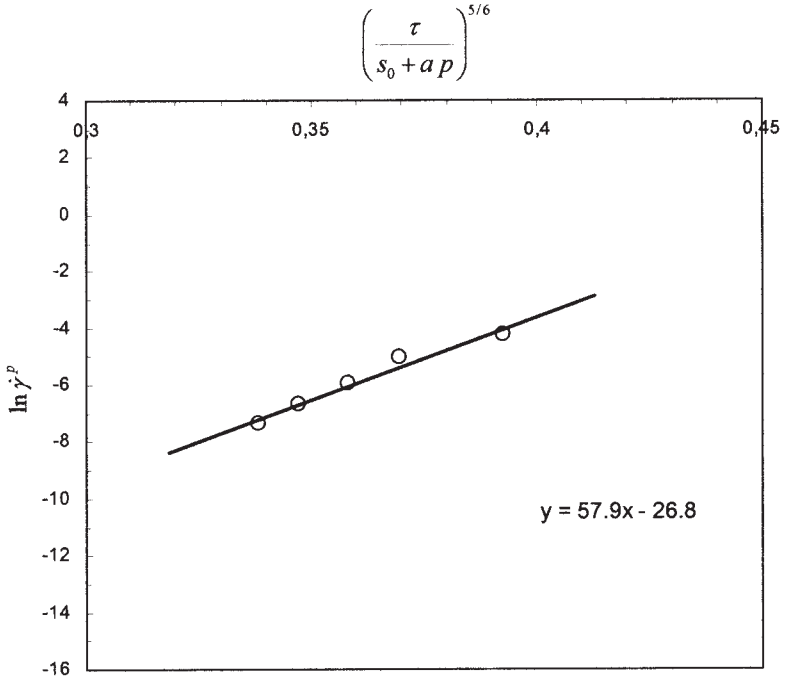

(a)

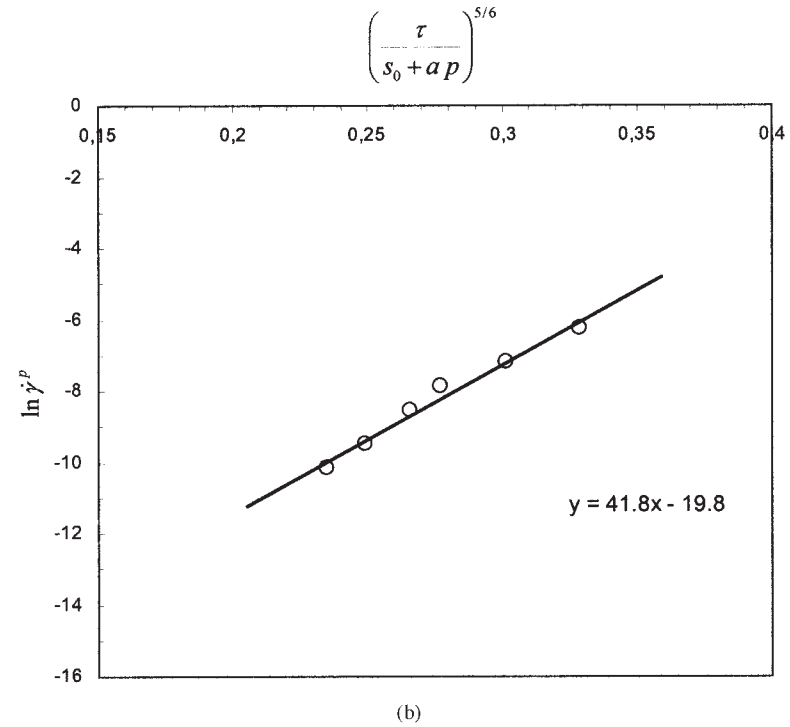

(b)

Figure 5 (a) Diagram of the approximation of A and $\dot{\gamma}_0$ coefficients of the BPA model from tension loading results. (b) Diagram of the approximation of A and $\dot{\gamma}_0$ coefficients of the BPA model from compression loading results.

The description of strain hardening at the last stage is introduced through the Langevin spring. In our case we will follow the three-chain model of James and Guth[12] (an interesting alternative approximation could be the model of eight chains of Arruda and Boyce[13] or the full-chain model of Wu and van der Giessen [14]). According to James and Guth[22] the principal back stresses in three dimensions will be given from the consequence relations

$$B_i = C^R \frac{\sqrt{N}}{3}\left[V_i^p L^{-1}\left(\frac{V_i^p}{\sqrt{N}}\right) - \frac{1}{3}\sum_{j=1}^{3} V_j^p L^{-1}\left(\frac{V_j^p}{\sqrt{N}}\right)\right], \quad (38)$$

TABLE III
Mechanical Properties and Constants for the BPA Model

	$\dot{\gamma}_0$ (/s)	A (K/MPa)	ε_y	t_y (s)	E (GPa)	E_1 (GPa)	E_2 (GPa)	T (K)	ν	α	C_r (MPa)	N	h (MPa)	s_{ss}/s_0
Tension/	4×10^7	78.4	0.045	50	3.1	0.2E	0.8E	295.5	0.394	0.231	9	2	1100	0.825
Compression	3×10^{15}	130											600	

Note. Where $t_y = E_1/\eta_1$ and $\varepsilon_y = \dot{\varepsilon}_0 E_2/\eta_2$.

where L^{-1} is the inverse Langevin function and V_i^P is the principal plastic stretching.

The material variables that are required for the approximation of entropic resistance is the rubber modulus C^R and the number of rigid links N between entanglements or crosslinks. The modulus C^R could be found, estimating the number of molecular segments n per volume unit in this specific temperature and using the following relation:[2,11]

$$C^R = nkT = \frac{\rho RT}{M_c}. \tag{39}$$

Through the stereochemical form of epoxide resin (Fig. 1), we could calculate their molecular weight M_c. So the preceding relation results easily to the value

$$C^R \sim 9 \text{ MPa}. \tag{40}$$

The number of rigid links N between entanglements or crosslinks could be calculated through tension tests as the limiting stretching of material. For the Langevin distribution N is equal to the square of limiting stretching λ_0. Due to the reduced ductility of the material during the tension test we could alternatively[15] estimate N one more time thought stereochemical form of epoxy resin, from which could be extracted (see Fig. 1) the value 2.

The magnitudes of quantities as were calculated for this specific material in the case of tension and compression loadings are presented in Table III.

Summarizing all previous results, a complete approximation of stress–strain response can be obtained. The Argon relation is selected for the description of yield stage with stress drop and dependence with pressure, whereas for the stage of strain hardening the Wang and Guth formalism is selected. Moreover, the use of a simple Hookean spring for the description of initial part of curve could give a good approximation of the magnitude of yield stress both in tension and in compression. But this ceases to happen for the initial viscoelastic stage and for yield strain, because they exhibit large diversions from experimental findings in both cases.

An important improvement is expected to arise using a viscoelastic analog instead of the simple Hookean spring. The introduction of Maxwell analog—with an elastic spring E and a viscous dashpot η—in this specific model improves most the results in the initial part of curve. Generally, a better efficiency of initial viscoelastic area and better approximation of yield strain appear, even though great diversions are discerned for low strain rates because the use of a simple relaxation time couldn't simulate exactly experimental results.

The introduction of a greater number of elements in the viscoelastic models used could lead to a better description. So, the efficiency of the BPA model, as we expected, is enhanced noticeably with the introduction of three parametric and a four parametric standards[16] with corresponding constitutive equations,

$$\sigma + \tau \frac{d\sigma}{dt} = E_a \varepsilon + (E_m + E_a)\tau \frac{d\varepsilon}{dt}, \tag{41}$$

(standard linear solid)
where

$$\tau = \frac{\eta_m}{E_m} \tag{42}$$

and

$$\sigma + (\tau_1 + \tau_2)\frac{d\sigma}{dt} + \tau_1\tau_2 \frac{d^2\sigma}{dt^2} = \frac{d\varepsilon}{dt}(\eta_1 + \eta_2) + (\tau_1\eta_2 + \tau_2\eta_1)\frac{d^2\varepsilon}{dt^2}, \tag{43}$$

(four parametric model—composed of springs E_i and dashpots η_i—with a liquid like character)
with

$$\tau_1 = \frac{\eta_1}{E_1} \quad \text{and} \quad \tau_2 = \frac{\eta_2}{E_2}. \tag{44a,b}$$

An even better approximation of the real viscoelastic phenomena could be obtained with a theoretical infinite number of spring elements and dashpots using a generalized Maxwell element and a generalized Voigt element. All the parameters values with a four parametric model are given in Table I and the stress–strain curves that we get from the above model are shown in Figure 6a and b for tension and compression, respectively.

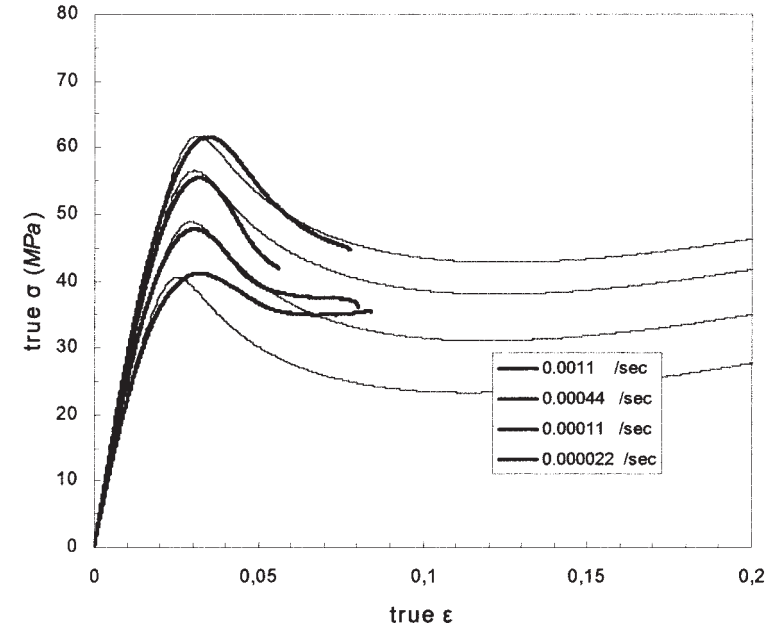

(a)

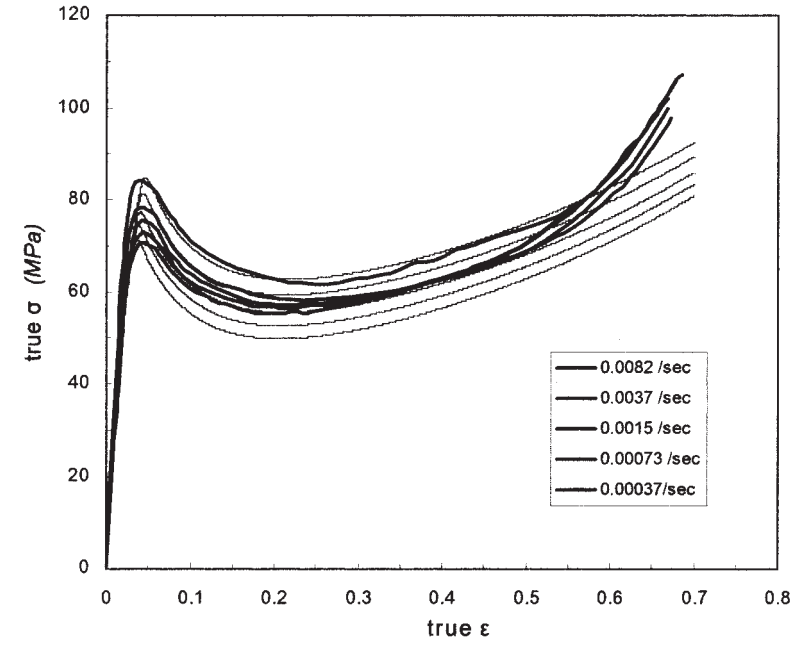

(b)

Figure 6 (a) The approximation of stress–strain curves with the Boyce–Parks–Argon model and using the four-parametric analog for the initial part of the curves. Unidirectional tension loading. (b) As in (a) but for unidirectional compression loading.

G'Sell and Jonas' constitutive model[10]

In the previous presentation the variation of plastic strain is considered a predominantly activated rate process where the observed strain rate changes exponentially with the imposed stress. A further assumption could be done regarding the density of the actual plastic sites with varying stress and specifically to a first approximation that it is changing linearly with the emergence of strain.

So, according to the consideration of G'Sell and Jonas the total strain ε is analyzed in three components:

$$\varepsilon = \varepsilon_{el} + \varepsilon_{vis} + \varepsilon_{pl}. \tag{45}$$

The viscoelastic component ε_{vis} could be approximated first through a Kelvin–Voigt model from which it is deduced that

TABLE IV
Mechanical Properties and Constants for G'Sell and Jonas' Model

	a (MPa)	b (MPa)	ε_c	w/kT (m^3/MJoule)	T (K)	E (GPa)	ν	a	C_r (MPa)	N
Tension/ Compression	6.5 4	105 100.3	3.2	0.04	295.5	3.1	0.394	0.231	9	2

$$\frac{d}{dt}\varepsilon_{vis} = \frac{\left(\frac{\sigma}{E_\nu} - \varepsilon_{vis}\right)}{\tau_R}, \tag{46}$$

where τ_R is the mean retardation time and E_v is the relaxation modulus.

The component of rate of plastic strain ε_{pl} following an analysis similar to metals is given generally from the Orowan relation,

$$\dot{\varepsilon}_{pl} = \rho(\sigma^*, \varepsilon) \cdot \upsilon(\sigma^*) \cdot \bar{b}, \tag{47}$$

where ρ is the mean length of plastic waves, υ is the mean velocity of propagation of waves, and $\bar{b}$ is the mean displacement of elementary local shearing. If we make the assumption that the nucleation and/or propagation of waves are activated rate processes and also that the density of plastic waves could be increased gradually as the deformation proceeds, in a first approximation this increase of wave density should change linearly up to a point (strain) of equilibrium establishing. Then the following relation for plastic strain rates is extracted,

$$\dot{\varepsilon}_{pl} = \dot{\varepsilon}_1 \exp\left[\frac{w(\sigma^* - \sigma_1^*)}{kT}\right] \cdot \frac{\varepsilon}{\varepsilon_c}, \tag{48}$$

(where σ^* and σ_1^* will be defined in Eqs. [52], [53], and [54].

In the preceding expression, it was considered that at the transition stage the variation of density of the generated plastic events is given by

$$\rho' = \rho \frac{\varepsilon}{\varepsilon_c} \quad (\text{for } \varepsilon < \varepsilon_c) \tag{49}$$

and

$$\rho' = \rho \quad (\text{for } \varepsilon \geq \varepsilon_c). \tag{50}$$

In this model the elastic component of the rubber behavior of polymer during the hardening stage is given in a similar way as in the BPA model. The dependence of yield stress on strain rate is attributed through the Eyring's relation, while the dependence of pressure is obtained through the corresponding dependence of athermal shear resistance. So, summarizing these remarks, the following system of differential equations is obtained:

$$\dot{\varepsilon} = \dot{\varepsilon}_{el} + \dot{\varepsilon}_{vis} + \dot{\varepsilon}_{pl} \tag{51}$$

$$\dot{\varepsilon}_{pl} = \dot{\varepsilon}_1 \exp\left[\frac{w(\sigma^* - \sigma_1^*)}{kT}\right] \cdot \frac{\varepsilon}{\varepsilon_c} \tag{52}$$

$$\sigma_1^* = a \ln \dot{\varepsilon} + b \tag{53}$$

$$\frac{d\sigma}{d\varepsilon} = E\left\{1 - \exp\left[\frac{w(\sigma - \sigma_i - \sigma_1^*)}{kT}\right] \cdot \frac{\varepsilon_n}{\varepsilon_c}\right\} \tag{54}$$

and substituting the corresponding viscoelastic equations the following expressions result:

$$\frac{d\sigma}{d\varepsilon} = E\left\{1 - \exp\left[\frac{w(\sigma - \sigma_i - \sigma_1^*)}{kT}\right] \cdot \frac{\varepsilon_n}{\varepsilon_c}\right\} - \frac{\sigma}{\dot{\varepsilon}\tau_r} \tag{55}$$

(Maxwell)
or

$$\frac{d\sigma}{d\varepsilon} = E_1\left\{\left(1 + \frac{E_2}{E_1}\right) - \exp\left[\frac{w(\sigma - \sigma_i - \sigma_1^*)}{kT}\right] \cdot \frac{\varepsilon_n}{\varepsilon_c}\right\} - \frac{\sigma}{\tau_r\dot{\varepsilon}} + \frac{E_2\varepsilon_n}{\tau_r\dot{\varepsilon}} \tag{56}$$

(three parametric)

$$\sigma = \sigma_n\lambda \tag{57}$$

$$\sigma_i = C^R \frac{\sqrt{N}}{3}\left[V_i^p L^{-1}\left(\frac{V_i^p}{\sqrt{N}}\right) - \frac{1}{3}\sum_{j=1}^{3} V_j^p L^{-1}\left(\frac{V_j^p}{\sqrt{N}}\right)\right]. \tag{58}$$

So, the parametric values defined above are given in Table IV, and Figure 7a and b shows the theoretical stress–strain curves as obtained from the above set of equations with a three parametric standard solid.

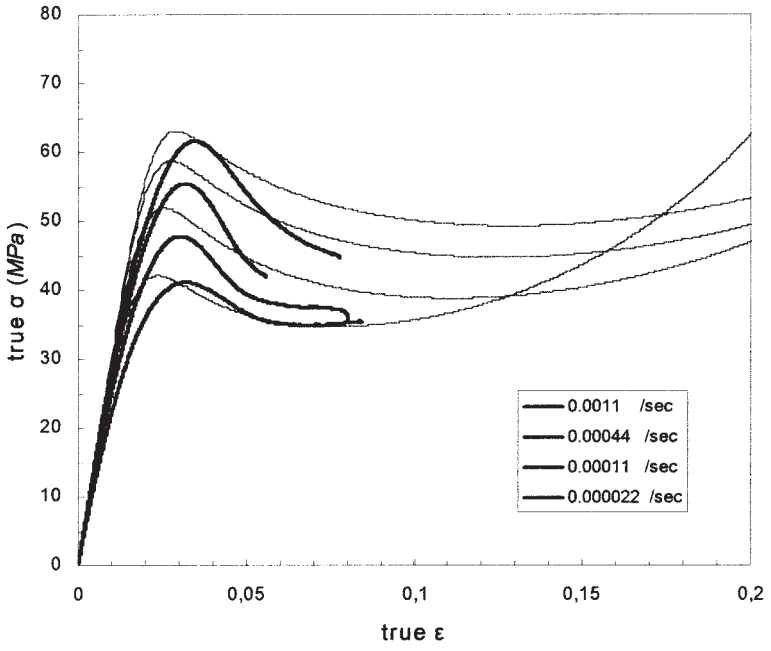

(a)

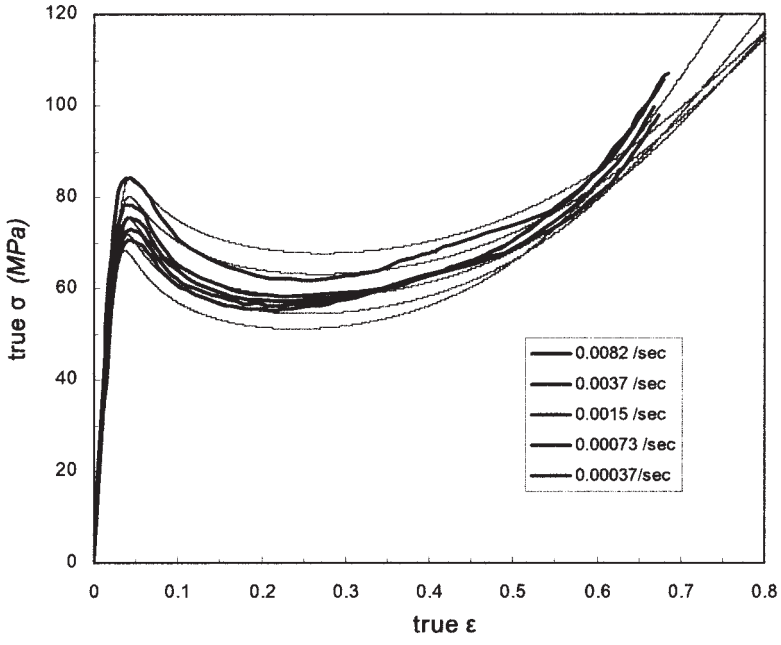

(b)

Figure 7 (a) The approximation of true stress–strain curves with G'Sell and Jonas' model using a three-parametric standard solid. Unidirectional tension loading. (b) As in (a) but for unidirectional compression loading.

Rubin's kinematics formulation of plastic behavior[17,18]

It has been made clear from many experimental observations such as in works by Oleinik et al.,[15] Argon,[8] and Hasan and Boyce,[19] that deformations in a viscoelastic material have an intensive inhomogeneous nature. But despite all these observations, mainly in the BPA model and partly in G'Sell and Jones' approximations, the main assumption of homogeneous deformation of materials has been made. An alternative way to include the observed inhomogeneity during deformation is the application of Rubin's approximation. Through this specific analysis it becomes possible, using microstructural material variables, to understand the expected mechanical response.

According to Rubin in the case of uniaxial experiment of an isotropic material the rate of elastic deformation $\dot{a}_m$ is given by the equation

$$\frac{\dot{a}_m}{a_m} = \left[\frac{1 + \frac{\mu}{3k}\left(\frac{a_m^3 - 1}{a_m}\right)}{1 + \frac{\mu}{9k}\left(\frac{5a_m^3 - 2}{a_m}\right)}\right]\left[\frac{\dot{a}}{a} - \frac{\dot{\gamma}^p}{18}\left(\frac{a_m^3 - 1}{a_m^3}\right) \times (4a_m^6 + 2)\right], \quad (59)$$

where a_m and $\dot{a}_m$ represent the elastic and the rate of elastic stretching, a and $\dot{a}$ are the total and the rate of total stretching, and $\dot{\gamma}^p$ is the rate of plastic deformation (Spathis and Kontou[20,21]). k and μ are the bulk and shear modulus, respectively.

If we adapt in this equation the micromechanical model for $\dot{\gamma}^p$ as introduced by Argon,

$$\dot{\gamma}^p = \dot{\gamma}_0 \exp\left\{-\frac{As_0}{T}\left[1 - \left(\frac{\tau}{s_0}\right)^{5/6}\right]\right\}, \quad (60)$$

and the additional equations for the rate of athermal shear resistance

$$\frac{d}{dt}s = h\left(1 - \frac{s}{s_{ss}}\right)\frac{d}{dt}\gamma^p \quad (61)$$

$$\tilde{s} = s(1 + ap/s) \quad (62)$$

with the constitutive equation of viscoelastic behavior

$$\sigma = E\varepsilon_y\left[1 - \exp\left(-\frac{a-1}{\varepsilon_y}\right)\right] \quad (63)$$

(Maxwell)
or

$$\sigma = E_1\dot{a}\tau_1\left[1 - \exp\left(-\frac{a_m - 1}{\dot{a}\tau_1}\right)\right] + E_2\varepsilon_y\left[1 - \exp\left(-\frac{a_m - 1}{\varepsilon_y}\right)\right], \quad (64)$$

(four-parametric)
where

$$p = \frac{1}{3}\,\mathrm{tr}\,\boldsymbol{T} \quad (65)$$

$$\tau = [\sigma - (B_1 - B_2)]/\sqrt{3} \quad (66)$$

$$B_1 = C^R\frac{\sqrt{N}}{3}\left[\lambda_p L^{-1}\left(\frac{\lambda_p}{\sqrt{N}}\right) - \frac{1}{3}\lambda_{p_j}L^{-1}\left(\frac{\lambda_{p_j}}{\sqrt{N}}\right)\right]$$

and

$$B_2 = C^R\frac{\sqrt{N}}{3}\left[1/\sqrt{\lambda_p}\,L^{-1}\left(\frac{1/\sqrt{\lambda_p}}{\sqrt{N}}\right) - \frac{1}{3}\lambda_{p_j}L^{-1}\left(\frac{\lambda_{p_j}}{\sqrt{N}}\right)\right],$$

the viscoplastic description of the deformed materials can be obtained. The solution of this set of equations is plotted in Figure 8a and b and the model parameters are given in Table V.

RESULTS AND DISCUSSION

In Figure 6a and b the stress–strain curves are presented following the BPA model where the four parametric description both for tension and for compression is also used. In this way, a satisfactory approximation to the experimental results is obtained. The strain rate effect and the effect of pressure in the stage of yield, the true strain softening, and that of hardening are also described.

Moreover, we go on to describe with good accuracy both the strain softening process and hardening. But this specific model couldn't give the dependence of the variation in stress drop with strain rate, exhibiting almost a constant percentage of stress drop after the yield point in all cases, as could be noticed directly in Figure 6, especially for the case of tension experiments. Also at hardening stage following experimental values, an inversion of the corresponding plots at different strain rates is observed. A satisfactory explanation for this kind of inversion is the adiabatic heating of specimens as the strain rate is increased, a situation that could be described accurately using this model and modifying appropriately the corresponding parameters.

Applying G'Sell and Jonas' description it is possible to obtain from the experimental data the ultimate value of strain under which an equilibrium in density of plastic waves is attained ($\varepsilon \sim 25$–30%). In this study we use the approximation of Gilman and Johnston of continually density increasing, a fact that didn't differentiate the whole procedure of approximation.

From the corresponding Figure 7a and b we see that G'Sell and Jonas' model, although it approximates the experimental results with a good accuracy with respect to the other two models, manages to attribute better all the revealing features: the viscoelastic part of the curve, variation of yield stress with strain rate and the stage of hardening, and the dependence of stress drop with strain rate.

Also through G'Sell and Jonas' model—and even more in Rubin's analysis—the stage after yield and mainly the stage of strain softening could be approximated, keeping in mind the inhomogeneous feature of deformation and avoiding the use of non full determine quantities like athermal shear resistance as in the BPA model.

Comparing now the results plotted in Figures 8a and b from Rubin's analysis with those in Figure 6a and b we conclude that a relatively small improvement was attained according to the corresponding analysis of BPA.

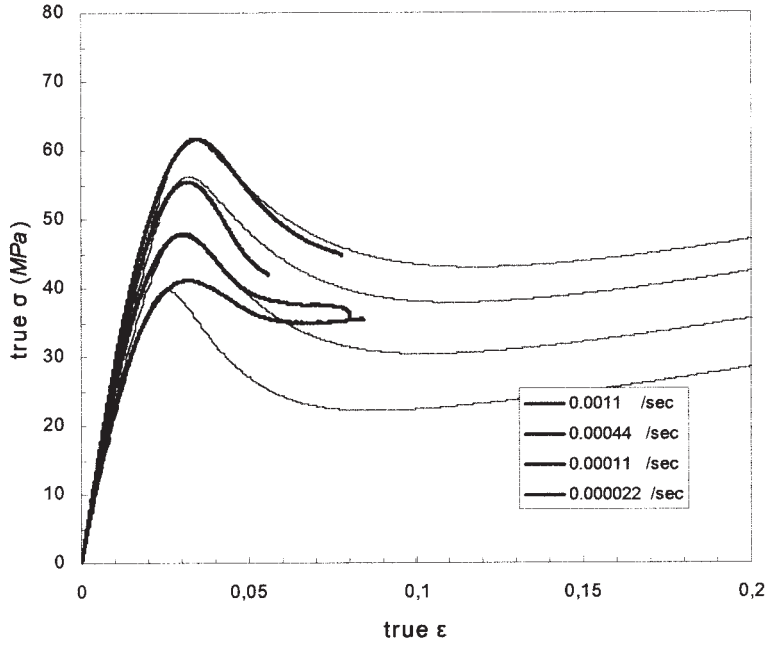

(a)

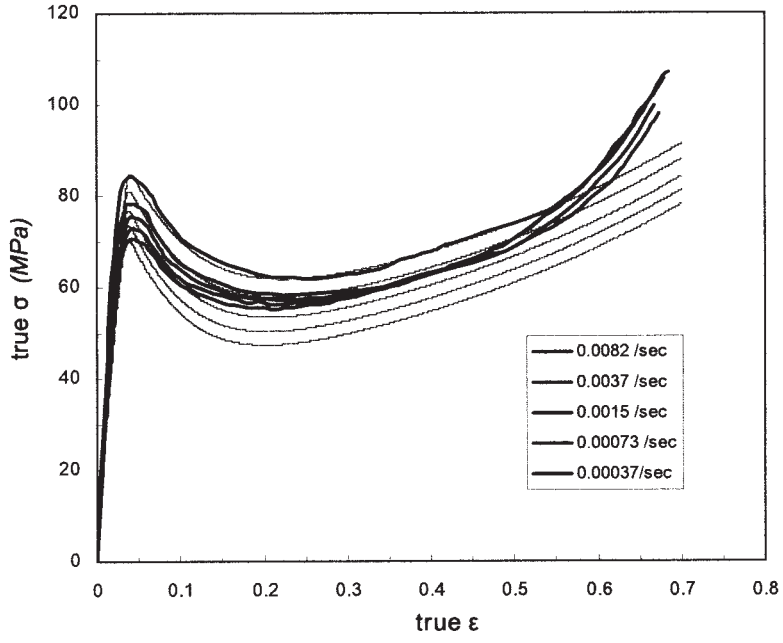

(b)

Figure 8 (a) The approximation of true stress–strain curves with Rubin's analysis using a four-parametric standard liquid. Unidirectional tension loading. (b) As in (a) but for unidirectional compression loading.

TABLE V
Mechanical Properties and Constants for Rubin's Model

	$\dot{\gamma}_0$ (/s)	A (K/MPa)	ε_y	t_y (s)	E (GPa)	E_1 (GPa)	E_2 (GPa)	T (K)	ν	α	C_r (MPa)	N	h (MPa)	s_{ss}/s_0
Tension/ Compression	1×10^8 6×10^{15}	72 123	0.045 0.06	50	3.1	0.2E	0.8E	295.5	0.394	0.231	9	2	60 35	0.83

Recapitulating the previous results, many interesting elements that concern the mechanical response of glassy polymers can be extracted.

At the initial stage of the stress–strain diagrams of glassy polymers the diversion from linear dependence is revealed; this fact could be attributed mainly to the appearance of viscoelastic events, which are magnified as the imposed stress increases. The use of linear viscoelastic models could sufficiently describe this behavior, but for detail countenance the use of nonlinear viscoelastic analysis is required. This diversion from linearity reaches a limiting situation where a maximum is observed. The existence of this maximum is connected with the appearance of viscoplastic deformations in material mainly localized in some regions of the specimen. A drop in demanding flow stress accompanies the revealing inhomogeneity. Depending now on the model used (Rubin, G'Sell–Jonas), this drop could be attributed to transition phenomena either of rearranging and reorientation of molecular chains (Rubin) or of a gradually increasing density of the appearing plastic shear transformations (G'Sell and Jonas).

Following the results contained in Tables III and V we can conclude that the values of h—a magnitude of the rate of strain softening—in the case of Rubin analysis appear to be mostly lower (35 to 60 MPa) than the corresponding values of the BPA approximation (600 to 1100 MPa). These decreasing until relatively zero values could indicate that the following kinematics is closer to the accurate representation of the predominant situation.

Based on relation (59) from Rubin's analysis,

$$\frac{\dot{a}_m}{a_m} = f(a_m)\left[\frac{\dot{a}}{a} - \Gamma g(a_m)\right], \qquad (59')$$

we can estimate the plastic multiplier Γ at equilibrium state,

$$\frac{\dot{a}_m}{a_m} = 0, \qquad (59a)$$

as

$$\Gamma \sim \frac{\dot{a}}{a}. \qquad (59b)$$

This result means that in the equilibrium state—peak of the yield limit—the rate of revealing plastic strain will be inversely proportional to the current deformation. Consequently, the drop in the plastic strain rate versus total deformation will cause a corresponding decrease in the required stress for continuing flow (G. Spathis, 2002). This conclusion, directly related to the kinematics description of Rubin's analysis, could help us to describe also the observable strain softening that the materials exhibit, possibly without the introduction of additional terms.

As far as the yield phenomenon is concerned, it seems plausible that an activated rate process is taking part and could be described equivalently either from the Eyring equation or the Argon relation where the logarithm of plastic strain rates in relaxation state is proportional to applying stress.

Finally, the stage of hardening of glassy polymers is approximated with high accuracy through a procedure proportional to the entropic hardening of rubbers, using mainly the relations of non-Gaussian distribution and the Langevin function.

CONCLUSIONS

The mechanical behavior of a polymer could be analyzed in viscoelastic, yielding, postyielding, and hardening stages. In this study we manage to describe these areas in a unique form. Using three different models we approximate the real response with good accuracy. The interesting point here was that the application of Rubin's kinematics seems to simplify the viscoplastic response of the polymer, probably showing a more realist description.

References

1. Crist, B. In The Physics of Glassy Polymers; Haward, R. N.; Young, R. J., Eds.; Chapman & Hall: London, 1997; p 155.
2. Ward, I. M. Mechanical Properties of Solid Polymers, 2nd ed.; Wiley: New York, 1983.
3. Aklonis, J. J.; MacKnight, W. J.; (M. Shen) Introduction to Polymer Viscoelasticity, 2nd ed.; Wiley: New York, 1983.
4. Matsuoka, S. Relaxation Phenomena in Polymers; Hanser: Munich, 1992.
5. Leonov, A. I. Rheol Acta 1976, 15, 85.
6. Trevoort, T. A.; Klompen, E. T.; Govaert, L.E. J Rheol 1996, 40, 979.
7. Bernstein, B.; Shokooh, A. J Rheol 1980, 24, 189.
8. Argon, A. S. Phil Mag 1973, 28, 839.
9. Bowden, P. B.; Raha, S. Phil Mag 1974, 29, 149.
10. G'Sell, C.; Jonas, J. J. J Mater Sci 1956, 1981, 16.
11. Boyce, M. C.; Parks, D. M.; Argon, A. S. Mech Mat 1998, 7, 15.
12. Boyce, M. C.; Haward, R. N. In The Physics of Glassy Polymers; Haward, R. N.; Young, R. J., Eds.; Chapman & Hall: London, 1997; p 213.
13. Arruda, E. M.; Boyce, M. C. J Mech Phys Solids 1993, 41, 389.
14. Wu, P. D.; van der Giessen, E. J. Mech Phys Solids 1993, 41, 427.
15. Oleinik, E. F.; Salamatina, O. B.; Rudnev, S. N.; Shenogin, S. V. Polym Sci 1992, 35, 1532.
16. Flugge, W. Viscoelasticity; Blaisdell: Waltham, MA, 1967.
17. Rubin, M. B. Int J Solids Struct 1994, 31, 2615.
18. Rubin, M. B. Int J Solids Struct 1994, 31, 2635.
19. Hasan, O. A.; Boyce, M. C. Polym Eng Sci 1995, 35, 331.
20. Spathis, G.; Kontou, E. J Appl Polym Sci 2007, 1999, 71.
21. Spathis, G.; Kontou, E. Polymer 1998, 39, 135.
22. James, H. M.; Guth, E. J Chem Phys 1943, 11, 455.
23. Spathis, G.; Kontou, E. Polymer Eng Sci 2001, 41, 1337.